JOURNAL OF APPLIED ELECTROCHEMISTRY 11 (1981) 573–582

# *The impedance of the alkaline zinc–mercuric oxide cell. I. Cell behaviour and interpretation of impedance spectra*

S. A. G. R. KARUNATHILAKA, N. A. HAMPSON, T. P. HAAS

*Department of Chemistry, University of Technology, Loughborough, Leicestershire, UK*

R. LEEK

*Department of Electronic and Electrical Engineering, University of Technology, Loughborough, Leicestershire, UK*

T. J. SINCLAIR

*Procurement Executive, Ministry of Defence, Royal Armament Research and Development Establishment, Fort Halstead, Sevenoaks, Kent, UK*

Received 28 October 1980

The impedances of small (2400 mA h) alkaline Zn–HgO cells have been measured in the range 10 kHz–0.001 Hz at various states of charge from fully charged to fully discharged. The behaviour of the cell conforms to that expected for rate control by charge transfer at the zinc electrode and diffusion in solution. At low frequencies there is a relaxation in the diffusive circuit elements which ultimately results in a complete suppression of the capacitative component of the impedance at zero frequency. The low-frequency behaviour is analogous to convective diffusion and is due to the effective distance between the electrodes being small compared with the characteristic length $(D/\omega)^{1/2}$. The magnitude of the charge transfer resistance is the best measure of the state of charge.

## Nomenclature

| | |
|---|---|
| $a$ | effective electrode separation |
| $C_{DL}$ | double-layer capacitance of cell |
| $C_R$ | capacitative component of cell impedance |
| $\Delta C$ | concentration difference |
| $D$ | percentage discharge in Equation 12 |
| $D_i$ | diffusion coefficient of species $i$ |
| $R_\Omega$ | ohmic resistance of cell |
| $R_R$ | resistive component of cell Faradaic impedance |
| $Ui$ | constant defined by Equation 10 |
| $Z$ | total cell impedance |
| $Z_F$ | cell Faradaic impedance |
| $Z'_F$ | cell impedance modified for porosity effect |
| $Z_X$ | cell impedance of Faradaic component plus double layer |
| $\sigma$ | cell Warburg coefficient (slope of $R_R$ and $1/\omega C_R$ versus $\omega^{-1/2}$) |
| $\sigma_C$ | Warburg coefficient calculated from $C_R$ values |
| $\sigma_i$ | cell Warburg coefficient for species $i$ |
| $\sigma_R$ | Warburg coefficient calculated from $R_R$ values |
| $\phi$ | dihedral angle of tail of Sluyters plot (after 'coming-off' high-frequency semi-circle) |
| $\omega$ | angular frequency |

## 1. Introduction

We have recently reported on the impedance of small primary cells of both the Leclanché type and the alkaline Zn–$MnO_2$ type [1–4]. We have shown that using an automatic technique for impedance measurement sufficient data can be obtained in a reasonable time for investigations of the kinetics to be made and the quantity of electricity remaining in the cell to be estimated. This

0021–891X/81/050573–09$02.90/0  

latter quantity can be estimated to a reasonable degree of accuracy by means of a simplified test based on a limited number of impedance readings [3]. The Leclanché cell proved to be much more amenable to this approach than the alkaline Zn–$MnO_2$ cell [4]; however, it is still an important objective of the present research to perfect a method of state-of-charge measurement for the case of the alkaline Zn–$MnO_2$ cell using a simple measurement.

We now wish to report the results of our investigations of the impedance of the alkaline Zn–HgO cell (the Mallory cell). The overall reaction for the alkaline Zn–HgO cell is [5]

$$Zn + HgO \rightleftharpoons ZnO + Hg. \quad (1)$$

Tye [6] has considered the evidence for the actual kinetic processes occurring within the cell. For the positive electrode the electrode process is first the formation of a solution species, probably $Hg(OH)_2$

$$HgO + H_2O \rightarrow Hg(OH)_2 \quad (2)$$

followed by its migration to a conducting point in the 'positive mass' (HgO and graphite) where it is reduced to metallic mercury

$$Hg(OH)_2 + 2e \rightarrow Hg + 2OH^-. \quad (3)$$

Under conditions where the positive electrode limits the discharge, it has been suggested [7] that the limiting process is due to the reduction of the $OH^-$ concentration so that the solution-soluble mercury species is present at too low a concentration to sustain the electrode reaction. Tye [6] considers that it is simply the concentration of Hg(II) species falling to zero at the charge transfer point. It is unlikely, however, that charge transfer at the positive electrode controls the total overpotential of the cell system, for the Hg(II)/Hg electrode is likely to be reversible. It is clear that the zinc electrode in alkali is not reversible [8] and, moreover, whereas the end product of the positive electrode reaction is highly conducting mercury, that of the negative is insulating zinc oxide. The net effect of these factors is that it is the negative electrode which determines the time of the reaction and largely controls the cell overvoltage and the cell impedance. This state of affairs was found to obtain in the alkaline Zn–$MnO_2$ cell and the impedance behaviour of this cell could be interpreted quite well in terms of the Zn electrode [4]. It is of interest to see if the alkaline Zn–HgO cell behaves similarly.

## 2. Experimental

The cell investigated was the RM502R (Mallory Batteries Ltd) which has a nominal capacity of 2400 mA h at room temperature. The cell was 50 mm in height and 14.2 mm in diameter. The initial open-circuit voltage was 1.35 V. The cell is contained in a corrosion-resistant, nickel-plated steel can. The positive electrode is a compressed mixture of HgO and graphite which increases the conductivity of the HgO phase; after a period of discharge the metallic Hg formed is sufficient to maintain the conductivity. The form of the positive electrode is a cylinder which is separated from the negative by a synthetic absorbent separator. The negative electrode is powdered zinc formed into a paste with alkaline potassium zincate and a binder. As with the alkaline Zn–$MnO_2$ cell [4] it is not possible to study either electrode separately as we did with the Leclanché cell because of the physical instability of the cell elements.

The experimental apparatus and procedure have been described before [1]. Cells were tested in quadruplicate, being chosen at random from a batch immediately after manufacture†. Cells were discharged galvanostatically at a rate of 24 mA and the impedance measured at various states-of-charge until 2400 mA h had been drained from the cell. The impedance data were obtained as a set of Sluyters plots and also put on to punched tape and read into a computer.

## 3. Results and discussion

Fig. 1 shows the Sluyters plot corresponding to a cell 'as-received' from the manufacturer. The shape consists of a high-frequency semicircle with a tail initially coming off at a dihedral angle of 38° which curves over and tends towards the real axis at $< 10$ mHz. This curve is almost exactly what would be expected from a simple charge transfer reaction at a moderately porous electrode

† We are grateful to Dr John Crofts and Mallory Batteries Ltd for arranging this and for the gift of the cells.

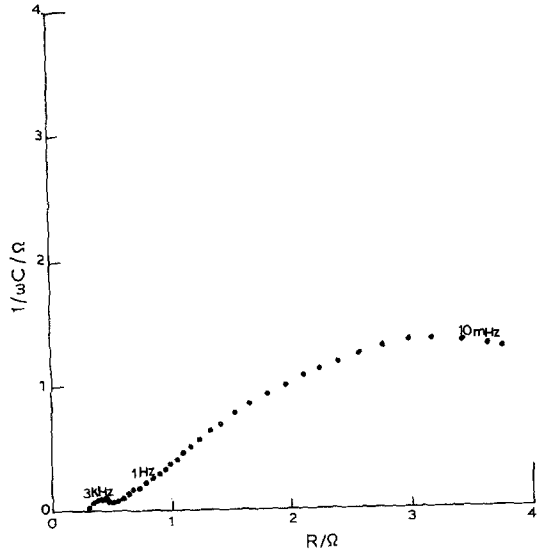


Fig. 1. Complex-plane plot for as-manufactured alkaline Zn–HgO cell. 22° C; zero current density.

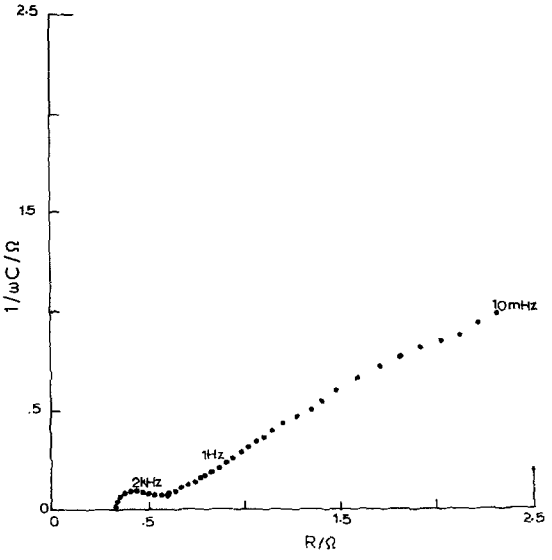


Fig. 2. As Fig. 1 but 1% discharged.

followed by diffusion in solution and tending towards a convective diffusion, mass transport limited, steady state. The limiting dihedral angle for an electrode with semi-infinite pores is $22\frac{1}{2}°$ and the greater slope expresses the fact that the electrode is not completely porous.

Confirmation that it is the zinc electrode which determines the cell impedance can be made if the present results are compared with that of the alkaline Zn–$MnO_2$ cell [4]. The behaviour is almost identical (same value of $\theta$ and dihedral angle), which (at least in the initial stages of discharge) forces the conclusion that this can only be if the zinc electrode controls the cell impedance behaviour. Further, for both types of cell there is the same tendency for the locus to return to the real axis at very low frequency. The slope of the tail $22.5° < \phi < 45°$ is interesting, for there is no doubt that the electrode is porous in the usual physical sense as it is made from discrete particles. Loss of porosity in the sense of de Levie [9] must be due therefore to the compacting process, the particles being forced together with considerable loss of voidage. The use of Hg to counteract the hydrogen evolution reaction would also tend to obscure porosity by providing a more 'liquid-like' surface.

Figs. 2–14 show the changes in the complex plane plot as the cell is progressively discharged to 100%. It is evident that no change occurs in the general shape of the impedance locus. However, the magnitude of the high-frequency semicircle increases, as indeed does the solution resistance $R_\Omega$ †. This is in agreement with the covering of the zinc electrode with a layer of zinc oxide which results in an effective reduction of the

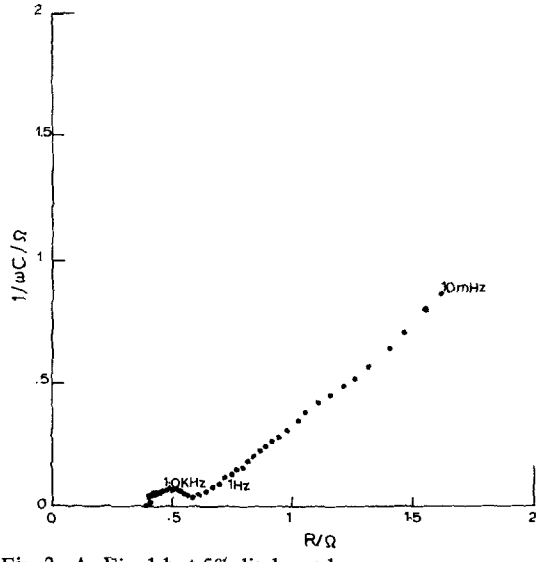


Fig. 3. As Fig. 1 but 5% discharged.

† The circuit elements of the cell contain uncertain area factors: we have avoided this problem throughout by considering the cell as it stands.

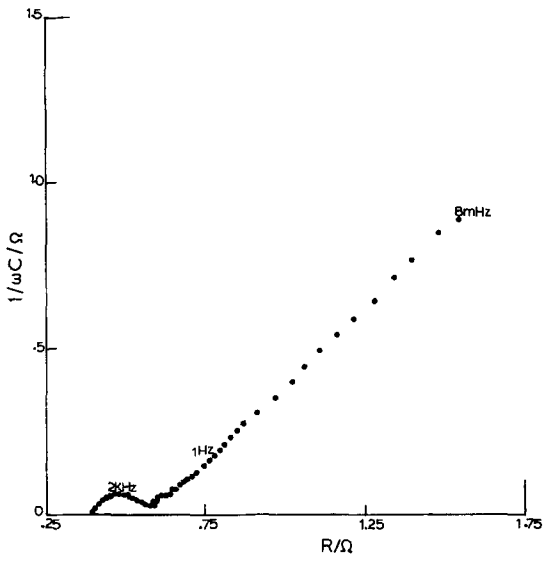


Fig. 4. As Fig. 1 but 10% discharged.

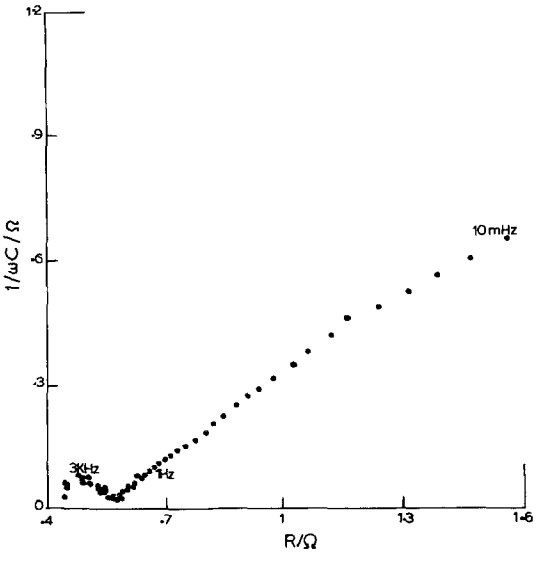


Fig. 6. As Fig. 1 but 20% discharged.

available surface area and also possibly reflects a reduction in the availability of the other electroactive component, the $OH^-$ concentration. The dihedral angle became closer to 45°, characteristic of a plane electrode, throughout this sequence. This can be interpreted as due to the electrode becoming more compacted because of the formation of ZnO (lower density than Zn) in the interstices of the electrode. It is further evidence that it is the zinc electrode which is being studied for there is no conceivable way in which the positive electrode could become less porous with discharging.

In this region of the charge (100–30%) the data were matched to a Randles-type circuit by finding the equation which fitted the impedance loci. In general it was not possible to fit all the data to the equations

$$Z_F = \theta + \sigma\omega^{-1/2} + i\sigma\omega^{-1/2} \quad (4)$$

$$\frac{1}{Z_X} = \frac{1}{Z_F} + i\omega C_{DL} \quad (5)$$

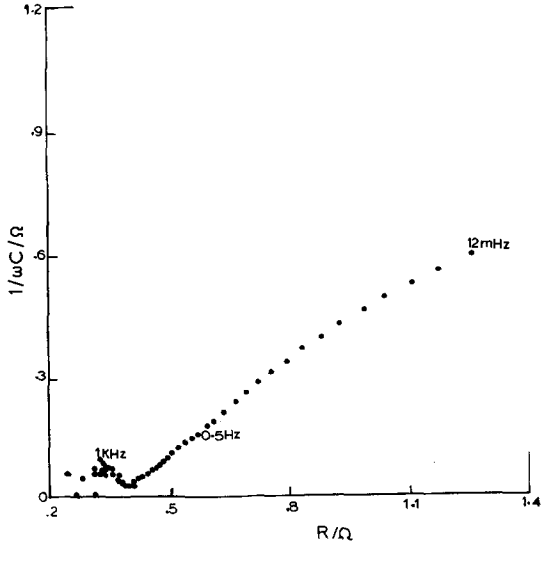


Fig. 5. As Fig. 1 but 15% discharged.

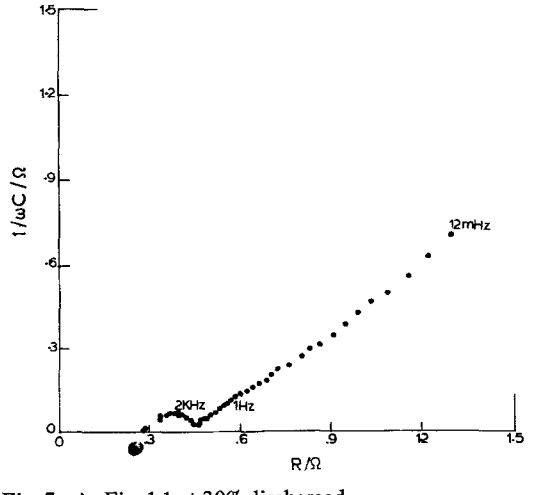


Fig. 7. As Fig. 1 but 30% discharged.

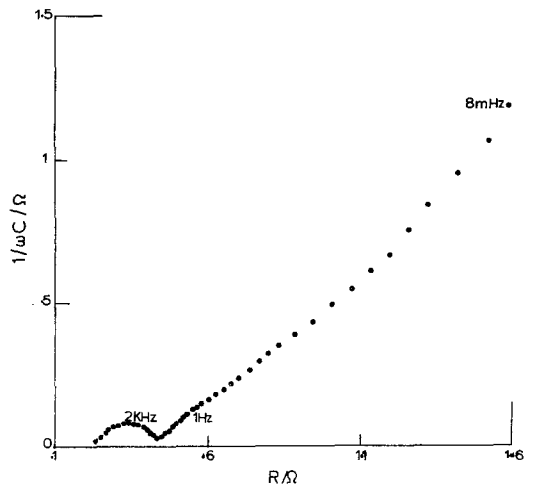


Fig. 8. As Fig. 1 but 40% discharged.

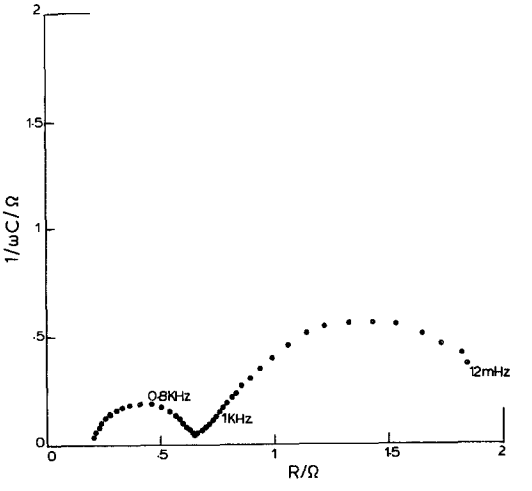


Fig. 11. As Fig. 1 but 70% discharged.

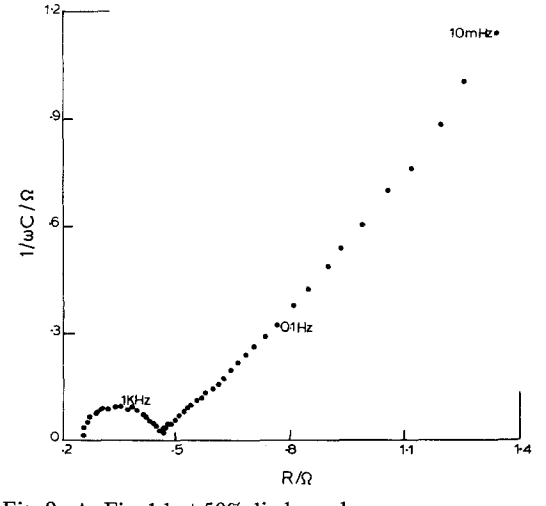


Fig. 9. As Fig. 1 but 50% discharged.

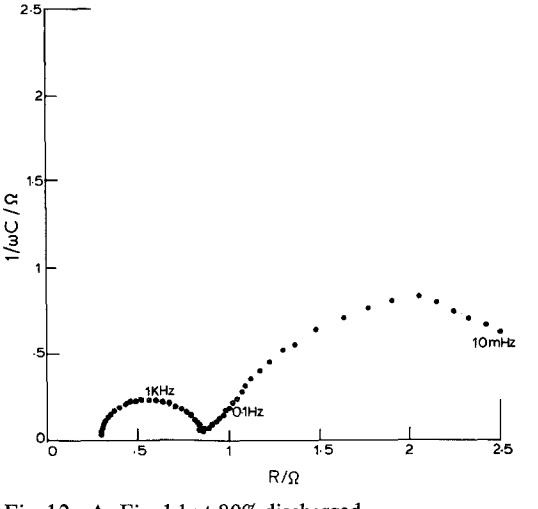


Fig. 12. As Fig. 1 but 80% discharged.

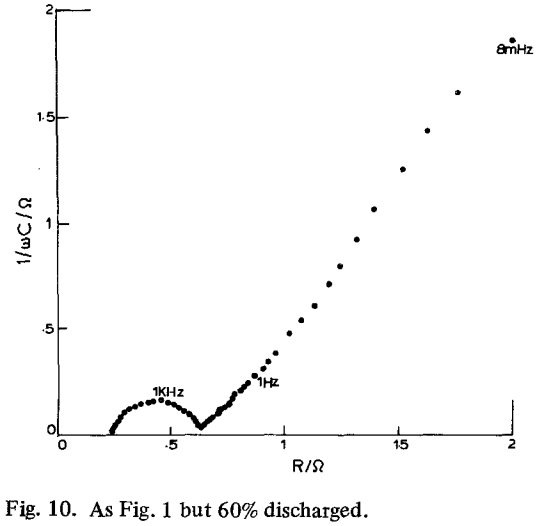


Fig. 10. As Fig. 1 but 60% discharged.

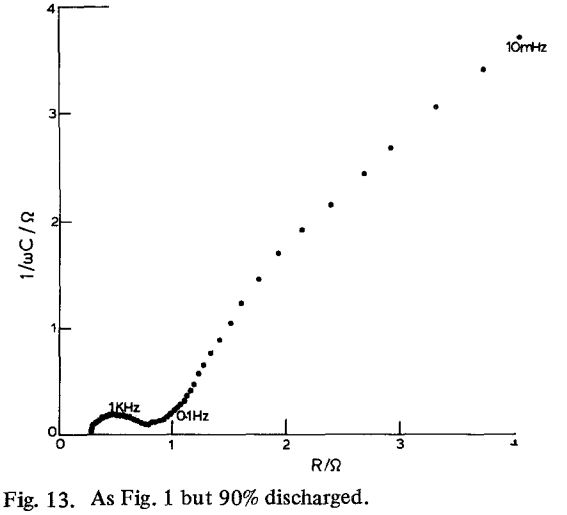


Fig. 13. As Fig. 1 but 90% discharged.

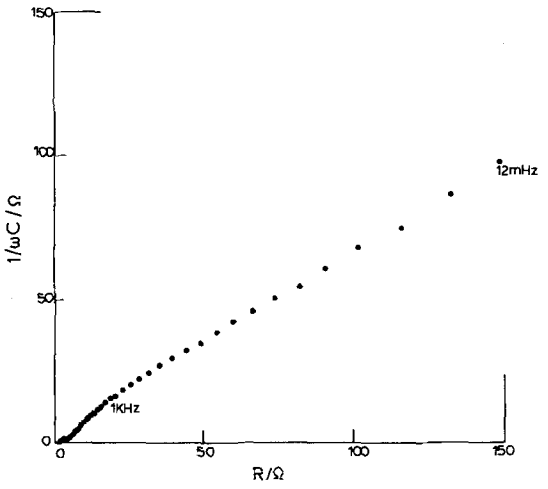


Fig. 14. As Fig. 1 but 100% discharged.

$$Z = Z_X + R_\Omega. \quad (6)$$

It was, however, found possible, with the aid of a computer, to fit those portions of the impedance plots generated before the curves begin to return the real axis by modifying Equation 4 to

$$Z'_F = \theta + \sigma_R \omega^{1/2} - i\sigma_C \omega^{-1/2} \quad (7)$$

where $\sigma_R$ and $\sigma_C$ are the slopes of the conventional Randles plot ($R_R$ and $1/\omega C_R$ versus $\omega^{-1/2}$), respectively, in the same limited range. Figs. 14–18 show that excellent correlations between theory and experiment can be obtained in a frequency range limited to 0.2 Hz. Table 1 shows the results obtained from the computations for states-of-charge in the range 100–0%.

The curvature of the lines at the lower frequencies is very interesting. A return to the real axis of the complex-plane representation is to be expected in the most general case of charge transfer and mass transport in solution when a convection-limited (steady-state) current results at long times when the control of the mass transport by diffusion in solution is superseded. In this present case the onset of convective control cannot be the cause of the curvature for the close packing of the components in the cell rules out the establishment of a convective field. Similarly, an explanation in terms of a porous or rough electrode is also inappropriate since, although the electrode is undoubtedly porous in the operational sense, the observed change in dihedral angle with frequency

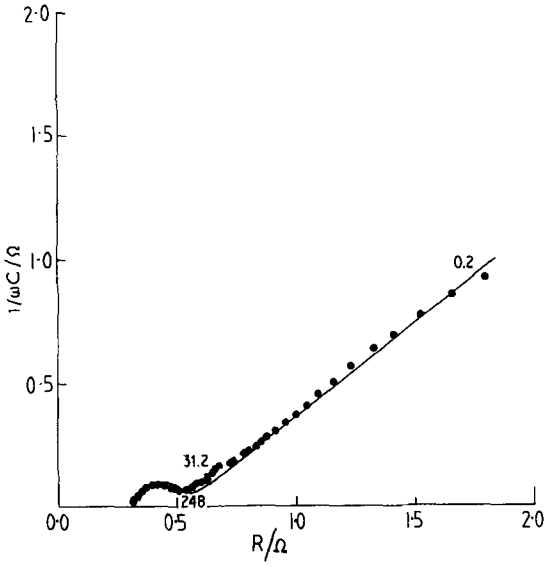


Fig. 15. Computer match of impedance data in frequency range 10 kHz–0.2 Hz. Data correspond to Fig. 1. •, experimental; — calculated.

would be expected to reach a limit at $22\frac{1}{2}°$ for an infinitely long pore. This is clearly not the case.

We consider that the reason for the return to the real axis is that the magnitude of the time available for diffusion between the two electrodes is becoming of the order of the period of the applied a.c. This will lead to a relaxation of the impedance with frequency since the boundary

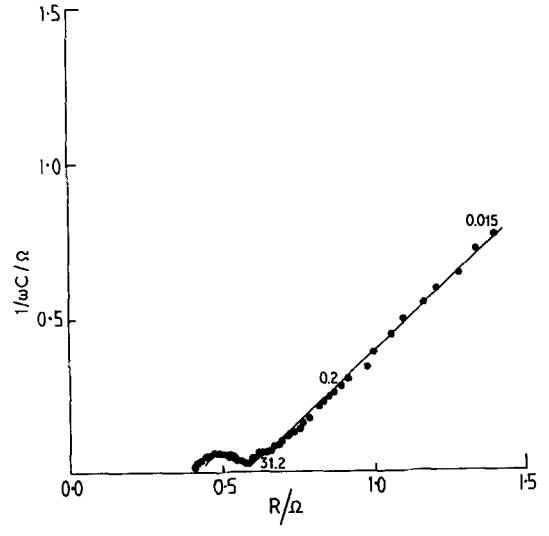


Fig. 16. As Fig. 15; data correspond to Fig. 4; 10 kHz–0.015 Hz.

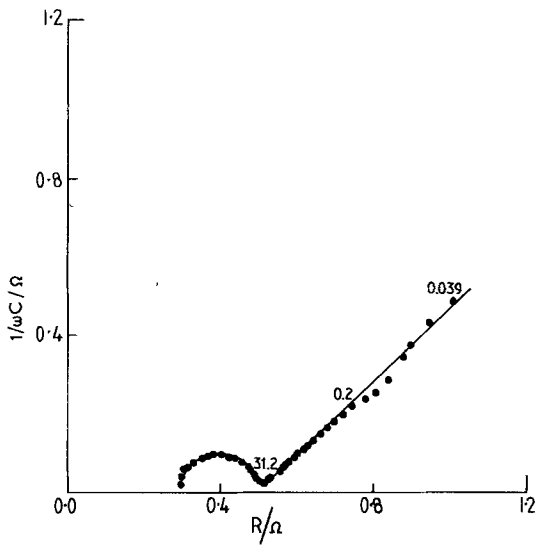


Fig. 17. As Fig. 15; data correspond to Fig. 9; 10 kHz–0.039 Hz.

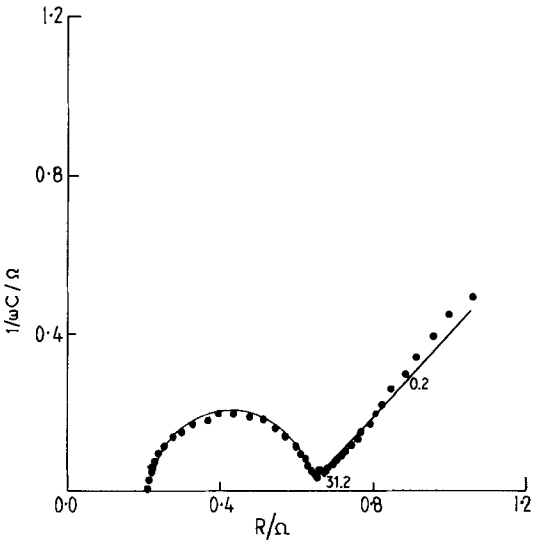


Fig. 18. As Fig. 15; data correspond to Fig. 12; 10 kHz–0.2 Hz.

condition that the concentration of the solution-soluble products falls to zero at points at an effectively infinite distance from the electrode cannot be maintained. This situation is one which is not uncommon in electrochemistry and has been made use of in principle in the various thin-layer techniques of electroanalytical chemistry [10–12]. The mass-transport problem here is very similar to that of the case for concentration diffusion [13] where the boundary condition is that $(\Delta C)_{x=a/2} = 0$, where $\Delta C$ is the a.c. component of the concentration and $a$ is the distance between the (identical) electrodes. In the present situation the primary Zn–HgO cell corresponds to

*Table 1. Parameters for a typical cell at various states of discharge*

| *State of discharge* (%) | $R_\Omega(\Omega)$ | $\theta(\Omega)$ | $C \times 10^3$(F) | $\sigma_C(\Omega\ s^{-1/2})$ | $\sigma_R(\Omega\ s^{-1/2})$ |
|---|---|---|---|---|---|
| New | 0.34 | 0.12 | 0.82 | 1.20 | 1.39 |
| 1 | 0.37 | 0.12 | 0.91 | 0.30 | 0.38 |
| 2 | 0.36 | 0.12 | 0.74 | 0.24 | 0.33 |
| 3 | 0.38 | 0.12 | 0.72 | 0.21 | 0.25 |
| 4 | 0.43 | 0.12 | 0.80 | 0.22 | 0.26 |
| 5 | 0.40 | 0.13 | 1.04 | 0.23 | 0.31 |
| 6 | 0.45 | 0.13 | 1.28 | 0.22 | 0.24 |
| 7 | 0.45 | 0.14 | 1.13 | 0.22 | 0.23 |
| 8 | 0.41 | 0.13 | 1.26 | 0.23 | 0.27 |
| 9 | 0.47 | 0.12 | 1.29 | 0.22 | 0.22 |
| 10 | 0.43 | 0.13 | 1.36 | 0.25 | 0.31 |
| 12.5 | 0.49 | 0.14 | 1.19 | 0.23 | 0.24 |
| 15 | 0.32 | 0.13 | 1.42 | 0.24 | 0.30 |
| 20 | 0.45 | 0.12 | 1.61 | 0.23 | 0.28 |
| 30 | 0.33 | 0.13 | 0.81 | 0.22 | 0.27 |
| 40 | 0.34 | 0.16 | 0.50 | 0.31 | 0.35 |
| 50 | 0.29 | 0.20 | 0.47 | 0.34 | 0.30 |
| 60 | 0.20 | 0.30 | 0.44 | 0.26 | 0.26 |
| 70 | 0.23 | 0.33 | 0.59 | 0.30 | 0.32 |
| 80 | 0.33 | 0.53 | 0.34 | 0.60 | 0.62 |
| 90 | 0.32 | 0.38 | 0.43 | 0.80 | 0.62 |

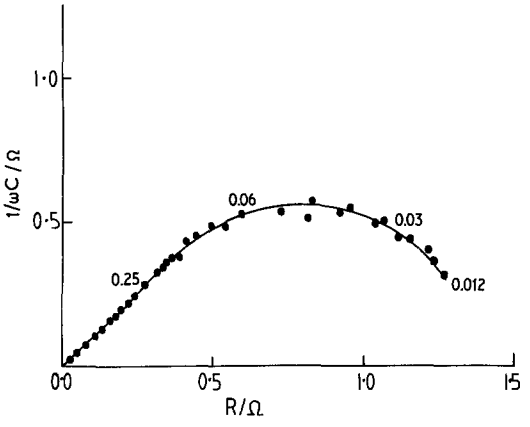


Fig. 19. The mass-transfer part of the cell impedance. Data as for Fig. 11, 70% discharged; 10 kHz–0.012 Hz.

a simple thin-layer cell provided that the species from the electroactive components do not leave their respective electrodes. Generally this is the case, for the electrode products ZnO and Hg remain at their respective electrodes. Under these conditions the transport of ($H^+$ and) $OH^-$ in an a.c. experiment provides ostensibly identical mass-transport processes at each electrode. In this case the mass-transport impedances are [14]

$$Z' = \sigma_i \omega^{-1/2} \left( \frac{\sinh(Ui) + \sin(Ui)}{\cosh(Ui) + \cos(Ui)} \right) \quad (8)$$

$$Z'' = \sigma_i \omega^{-1/2} \left( \frac{\sinh(Ui) - \sin(Ui)}{\cosh(Ui) + \cos(Ui)} \right) \quad (9)$$

$$Ui = (2a)^{1/2} \left( \frac{\omega}{D_i} \right)^{1/2} \quad (10)$$

where $D_i$ is the diffusion coefficient of the diffusing species, in this case $OH^-$. If the effective electrode separation is large by comparison with the

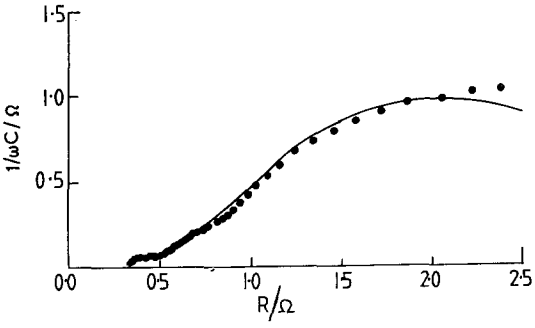


Fig. 20. Full line, computer match of impedance data using Equations 4–10; •, data as for Fig. 1.

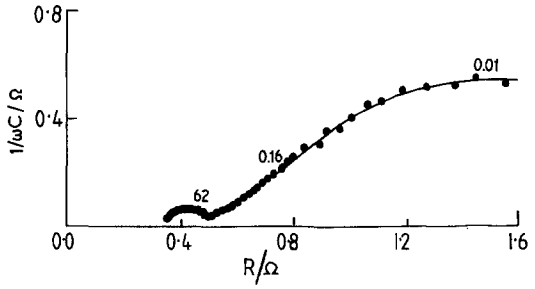


Fig. 21. Computer match as Fig. 20; data for 2% discharged cell.

characteristic distance $(\omega/D_i)^{1/2}$ then Equations 8 and 9 become identical with the $\omega^{-1/2}$ terms in Equation 4 and the dihedral angle is 45°; as $\omega$ is decreased the locus steadily returns to the real axis giving the intercept at $\omega = 0$

$$Z'_{F\omega \to 0} = \theta + \sigma_i \left( \frac{2a}{D_i} \right)^{1/2} \quad (11)$$

which is the d.c. current–voltage equation for the cell†.

This behaviour is essentially a relaxation, the out-of-phase component increasing and then decreasing to zero as the impedance locus oscillates around the straight line of slope 45° before returning to the real axis when $\omega$ becomes zero. It would appear from the construction of the cell, with electrodes separated by fibrous polyester material, that a clearly defined 'thin layer' cell is absent. However, this has been discussed by

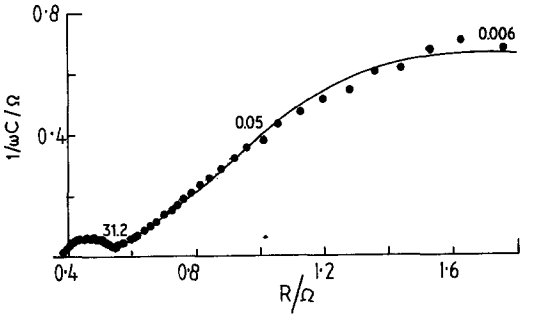


Fig. 22. Computer match as Fig. 20; data for 8% discharged cell.

† This is unlikely to be observed since under d.c. conditions continuous 'new phase' formation at the electrode intrudes. Under a.c. conditions it will be observed since no 'net' phase formation is involved.

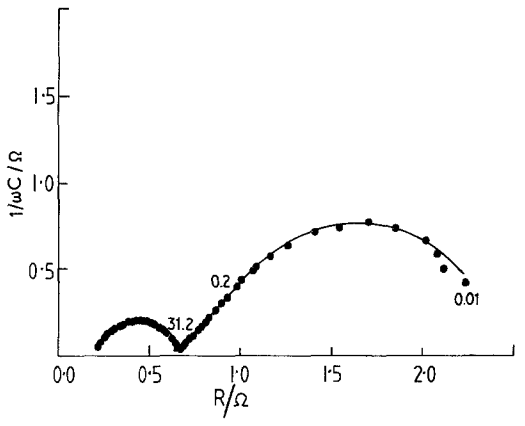


Fig. 23. Computer match as Fig. 20; data as Fig. 12.

Oldham and Tapol [15–17] where it is clear that if sufficient of the electrolyte solution volume is replaced by an inert porous media then the situation becomes that of the thin-layer cell.

We have tested the validity of the argument by isolating the mass-transport components of the cell impedance by subtracting from the total cell impedance, $R_\Omega$, $C_L$ and $\theta$ obtained from the computer. This was then matched with the theoretical Equations 8–10 assuming $D_i$ and estimating $a$ as a consequence. The results of a typical decomposition are shown in Fig. 19 which, with $D_i = 3 \times 10^{-5}$ cm$^2$ s$^{-1}$ give $a$ as 0.017 cm, a very reasonable value.

Figs. 20–23 show that the curvature can be taken into account at the lower frequencies if Equations 8 and 9 are used. In the present case it is possible to ascribe quite definite values to $a$, the semi-electrode separation distance. This is of course an average figure and must contain some contribution from the porous media. Values of these electrode separations are given in Table 2.

The change in impedance with state-of-charge

*Table 2. Typical values of a*

| *Discharge (%)* | *Cell number* | *a*(cm) |
|---|---|---|
| 0 | 3 | 0.076 |
| 2 | 3 | 0.021 |
| 8 | 3 | 0.028 |
| 20 | 2 | 0.015 |
| 60 | 2 | 0.015 |
| 70 | 2 | 0.017 |
| 70 | 3 | 0.022 |
| 80 | 2 | 0.020 |

*Table 3. Typical correlation coefficients for various cell impedances with state-of-charge throughout frequency range*

| *Frequency* | *Correlation coefficient with state-of-charge of 1–10%* | | |
|---|---|---|---|
| (Hz) | *Z'* | *Z''* | *Z* |
| 9900 | 0.713 | 0.730 | 0.706 |
| 1241 | 0.538 | 0.697 | 0.511 |
| 124 | 0.144 | 0.744 | 0.120 |
| 12.4 | 0.178 | 0.770 | 0.346 |
| 1.24 | 0.509 | 0.852 | 0.571 |
| 0.124 | 0.628 | 0.885 | 0.697 |

was investigated in the same way as with the Leclanché and the alkaline zinc–manganese dioxide cells. Table 3 shows the results of the correlations, which are far too weak to serve as a suitable indication. However, the diameter $\theta$ of the high-frequency semicircle changed steadily with the state-of-charge. This was an increase in the diameter (the charge-transfer resistance) and Fig. 24 shows the effective rate constant $(1/\theta)$ plotted against the state-of-charge. If the effective charge transfer resistance were determined by the 'concentration' of some electroactive species then a $\theta$ versus log (% charge) plot would be expected and if the peripheral surface area of the undischarged electroactive surface determined $\theta$ then $\theta^{-2}$ should strongly correlate with the percentage charge. The best fit obtained suggests that the available surface is steadily being covered with blocking products (or that the electroactive com-

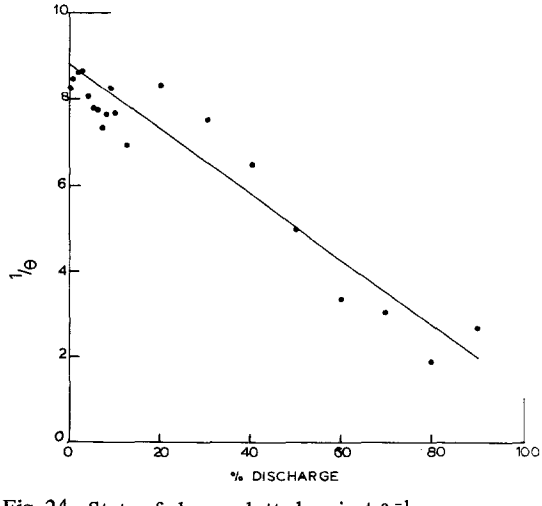


Fig. 24. State-of-charge plotted against $\theta^{-1}$.

ponent is being steadily removed) as the process proceeds.

The state-of-charge of the cell is given by the equation

$$1/\theta = -(0.76 \pm 0.04) \times \%D + (8.84 \pm 0.36). \quad (12)$$

## 4. Conclusions

(a) The impedance of the alkaline Zn–HgO cell is largely determined by the zinc electrode.

(b) The impedance spectra in the range down to 0.1 Hz are relatively simple indicating control by charge transfer and diffusion at a moderately smooth electrode.

(c) The state-of-charge of the cell is most readily given by the magnitude of $\theta^{-1}$.

(d) At low frequency the impedance relaxes due to the effective path length between the electrodes $a$ being of the order of $(D_{OH^-}/\omega)^{1/2}$.

## Acknowledgement

This work has been carried out with the support of Procurement Executive, Ministry of Defence.

## References

[1] S. A. G. R. Karunathilaka, N. A. Hampson, R. Leek and T. J. Sinclair, *J. Appl. Electrochem.* **10** (1980) 357.
[2] *Idem, ibid* **10** (1980) 608.
[3] *Idem, ibid,* **10** (1980) 799.
[4] *Idem, ibid,* **11** (1981) 365.
[5] R. Huber, 'Trackenbatterien und Luftsanerstoffelmente', Varta Aktiengesellshaft, Hanover (1972) p. 111.
[6] F. L. Tye, in 'Electrochemical Power Sources', (edited by M. Barak) Peter Peregrinus for IEE, London (1980) Ch. 3, p. 50.
[7] E. A. Mendzheritskii and V. S. Bagotski, *Electrokhem.* **2** (1966) 1312.
[8] N. A. Hampson, 'Silver Oxide–Zinc Batteries', (edited by J. J. Lander and A. Fleischer) John Wiley, New York (1971) Ch. 5.
[9] R. de Levie. *Adv. Electrochem. Electrochem. Eng.* **6** (1967) 329.
[10] B. R. Christensen and F. B. Anson, *Anal. Chem.* **35** (1963) 205.
[11] *Idem, ibid,* **36** (1964) 495.
[12] *Idem, ibid* **36** (1964) 732.
[13] J. H. Sluyters, *Rec. Trav. Chim.* **82** (1963) 100.
[14] For an excellent collected account of these effects the reader is referred to M. Sluyters-Rehbach and J. H. Sluyters, 'Sine Wave Methods in the Study of Electrode Processes', in *Adv. Electroanal. Chem.* No. 4 (edited by A. Bard) Marcel Dekker, New York (1971) Ch. 1.
[15] K. B. Oldham and L. E. Tapol, *J. Phys. Chem.* **71** (1967) 3007.
[16] *Idem, ibid* **73** (1969) 1455.
[17] *Idem, ibid* **73** (1969) 1462.